Ab initio Energies and Product Branching Ratios

for the O + C$_3$H$_6$ Reaction

Gary D. DeBoer

Department of Chemistry and Physics, LeTourneau University, Longview, TX 75602

James A. Dodd*

Air Force Research Laboratory/Space Vehicles Directorate, Hanscom AFB, MA 01731-3010

*Corresponding author. E-mail: James.Dodd@hanscom.af.mil.

Abstract

Intermediate and transition state energies have been calculated for the O + C$_3$H$_6$ (propene) reaction using the compound *ab initio* CBS-QB3 and G3 methods in combination with density functional theory. The lowest lying triplet and singlet potential energy surfaces of the O-C$_3$H$_6$ system were investigated. RRKM statistical theory was used to predict product branching

fractions over the 300-3000 K temperature and 0.001-760 Torr pressure ranges. The oxygen atom adds to the C_3H_6 terminal olefinic carbon in the primary step to generate a nascent triplet biradical, CH_3CHCH_2O. On the triplet surface unimolecular dissociation of CH_3CHCH_2O to yield $H + CH_3CHCHO$ is favored over the entire temperature range, although the competing $H_2CO + CH_3CH$ product channel becomes significant at high temperature. Rearrangement of triplet CH_3CHCH_2O to CH_3CH_2CHO (propanal) via a 1,2 H-atom shift has a barrier of 122.3 $kJ\,mol^{-1}$, largely blocking this reaction channel and any subsequent dissociation products. Intersystem crossing of triplet CH_3CHCH_2O to the singlet surface, however, leads to facile rearrangement to singlet CH_3CH_2CHO which dissociates via numerous product channels. Pressure was found to have little influence over the branching ratios under most conditions, suggesting that the vibrational self-relaxation rates for $p \leq 1$ atm are negligible compared to the dissociation rates.

I. Introduction

The gas-phase reaction of $O(^3P)$ with short-chain alkenes C_nH_{2n} is fundamental in physical chemistry and in combustion. Ethene, C_2H_4, is a key intermediate in the oxidation of CH_4 and longer-chain hydrocarbons.[1,2] The O-C_nH_{2n} system involves a large number of possible rearrangements, dissociations, and secondary reactions that can complicate determining the kinetic parameters and product species arising from the initial step. Mechanistically the basics of the $O + C_nH_{2n}$ reaction series are reasonably well understood, especially for the simplest case, $O + C_2H_4$. The O atom adds to the terminal olefinic carbon to form a triplet biradical RCH_2-CH_2O that undergoes rearrangement and/or dissociation involving a large number of reaction intermediates and transition states,[3-5] complicated by the presence of the lower-energy singlet surface accessible by intersystem crossing from the nascent triplet biradical. Experiments have shown that for the prototypical $O + C_2H_4$ system the initially-formed CH_2-CH_2O triplet biradical follows two principal reaction pathways: (1) direct dissociation to $H + CH_2CHO$, the vinoxy radical, and (2) intersystem crossing to form singlet CH_2-CH_2O, followed by 1,2 H-atom transfer and C-C bond cleavage to yield $CH_3 + HCO$.[3,4,6-8]

High-energy collisions of O with C_nH_{2n} species, among other small molecules and radicals, are also of increasing interest in the context of the near-space environment. Above 80 km altitude O atoms are prevalent in the atmosphere due to solar VUV photodissociation of O_2.[9] Collisions of O with molecular species associated with space vehicle operation in low-earth orbit can produce highly-excited, radiating products owing to very large relative collision velocities. For instance, collision of ambient O with desorbed H_2O from the Space Shuttle results in electronically-excited OH(*A*) giving rise to *A-X* emission in the near UV, and in physical excitation of several vibrational modes of H_2O resulting in emission in the 1.7-6.3 μm near- and mid-infrared spectral

region.[10]   For a satellite in a circular orbit at 300 km the orbital velocity is 7.726 km s^{-1}, corresponding to 3.59-eV center-of-mass collision energy for the $O + C_3H_6$ reaction assuming a stationary O atom. If thrusters are fired, the approximately 3.5 km s^{-1} exhaust velocity can add or subtract from the orbital velocity depending on the "attack angle" relative to the spacecraft orbit vector, giving rise to COM collision energies up to several eV larger.[11]   Partially- or unburned fuel constituents in thruster exhaust can result in efficient production of spectrally bright emitters upon reaction with O. Laboratory data confirming this effect have been obtained for collisions of hyperthermal O with CH_4,[12] C_2H_2,[13] hydrazines,[14] N_2,[15] and CO_2.[16]

Atomic oxygen has also been implicated in the degradation of low-earth orbit spacecraft surfaces.[11,17]   These effects can include inelastic scattering, chemical reactions with surfaces, surface-catalyzed reactions, and sputtering. For instance, osmium films, which are relatively inert for most ground-based applications, oxidize and degrade in low-earth orbit, releasing gaseous OsO_4. Hydrocarbon-based polymers are also slowly oxidized by impinging atomic oxygen to produce gas-phase metastables which could exhibit reactivity similar to the $O + C_nH_{2n}$ system. At the same time, surface imperfections such as scratches, pin defects and overall roughness can result in a drastically increased rate of degradation due to trapped oxygen atoms which can undercut an otherwise highly-protective surface coating.

The $O + C_nH_{2n}$ reaction for $n = 2$-4 has been studied in a number of laboratory experiments utilizing various techniques to form O atoms, notably discharge or Hg-sensitized flow[18-20] and laser photolysis of an NO_2 or SO_2 precursor.[21-24]   Using the latter technique, Bersohn and coworkers reported detailed product state results for the reaction of O with several alkenes in a series of landmark publications.[4,5,25-27] A number of crossed-beam experiments spanning almost four decades have also been reported.[6-8,28-32]   In terms of computation, the recent work of

Nguyen *et al.*[33] offers an excellent summary of the theoretical studies done on the benchmark $O + C_2H_4$ system, including the relatively recent calculation of the triplet surface.[34] The Nguyen *et al.* reference sets out a comprehensive high-level study of intermediate and transition state energies for the $O + C_2H_4$ system for both the triplet and singlet surfaces, and goes on to predict product branching ratios using RRKM unimolecular reaction rate theory.

Given the ongoing importance and rich chemistry inherent in the series of $O + C_nH_{2n}$ reactions, together with the large amount of experimental data, it makes sense to use currently-available computational tools to better understand the stationary states and likely reaction pathways following formation of the nascent triplet biradical. The Nguyen *et al.* theoretical study mentioned above demonstrates the tools and methods that can be applied to these systems. While that work focused on the prototypical $O + C_2H_4$ reaction, the existing information regarding the higher alkenes suggests that *ab initio* computations and RRKM theory be applied to longer-chain alkenes, to gauge the similarities and differences between the electronic structure and product state predictions. This work applies similar *ab initio* quantum mechanical calculations and RRKM unimolecular rate theory to the next larger system, $O + C_3H_6$.

II. Methodology

II.A Quantum chemistry models

The reaction system was modeled using the Gaussian 03 software package[35] running on a Pentium-based personal computer, together with GaussView for visualization. Three levels of calculation were pursued: density functional theory (DFT), and the compound complete basis set with quadratic configuration interaction (CBS-QB3)[36] and Gaussian-3 (G3)[37] *ab initio* methods. The DFT method was used to survey the potential energy surface (PES) through the calculation

of energies for intermediates and transition states, and to follow the internal reaction coordinate (IRC). The CBS-QB3 and G3 methods were used to obtain more accurate energies than those provided by DFT-level results. When possible, the average of the calculated CBS-QB3 and G3 energy values was input into the RRKM analysis, described below. The lowest lying triplet and singlet surfaces of the $O-C_3H_6$ system were investigated.

The Becke three-parameter/Lee-Yang-Parr density functional (B3LYP)[38] was used within the DFT approach, with unrestricted electron pairing on both the triplet and singlet surfaces. As discussed below, the B3LYP results provided important inputs for the higher-level methods. The method includes correlation interactions while running at a speed comparable to lower-level Hartree-Fock calculations. A 6-31+G(d,p) basis set was used in the B3LYP method for the initial survey. Energies for individual molecules were found using a geometry optimization. The sum of the energy of any two species, molecule, radical, or atom, was taken as the energy of the two species at infinite separation. All species were treated as neutrals.

The energy along the various reaction pathways was calculated by first locating a transition state. The transition state was found using the quadratic synchronous transit (QST2) method within Gaussian that requires input of reactant and product geometries and energies. The transition state was confirmed by checking that the resulting Hessian contained only one imaginary frequency, consistent with a first-order saddle point on the PES. To ensure that the transition state connected the assumed reactants and products, an IRC calculation was performed to follow the energy path from the transition state structure to the reactants and products located on opposite sides of the PES saddle point.

Intermediates and transition states that were amenable to the DFT method using the B3LYP/6-31+G(d,p) level of calculation in the initial PES survey were also examined at a higher

level of theory. The B3LYP method with a larger basis set, 6-311++G(3df,2p), was used to calculate species energies. The initial B3LYP/6-31+G(d,p) survey had found transition state geometries with enough accuracy that the "Berny" optimization method in Gaussian[39] could be employed successfully to obtain transition state structures at the B3LYP/6-311++G(3df,2p) level using the initial geometries from the B3LYP/6-31+G(d,p) calculation.

The compound CBS-QB3 method takes advantage of the initial B3LYP geometry survey to calculate more accurate energy values.[36,40] For finding minimum energy conformations the CBS-QB3 method can be run as a single job. For transition states the CBS-QB3 method was started at its second step, a second-order Moller-Plesset (MP2) single-point energy calculation, after reading in the results of a B3LYP/6-311G(2d,d,p) geometry optimization. The transition states calculated using the B3LYP/6-311++G(3df,2p) basis were reoptimized using the 6-311G(2d,d,p) basis, to be consistent with energy minima calculated using CBS-QB3/6-311G(2d,d,p). The results were then incorporated into the second step of the CBS-QB3 method.

The seven-step G3 prescription employs quadratic configuration interaction with single and double excitations and triple excitations added perturbatively (QCISD(T)).[37] Given that the G3 method involves a geometry optimization using a full MP2 step, it is well suited for the calculation of transition state energies and frequencies. To calculate transition state energies the G3 steps were run separately, starting with Hartree-Fock and MP2 transition state geometry optimizations followed by single-point calculations. The results of these calculations were then compiled to obtain the G3 transition state energies as outlined by Curtiss *et al.*[37]

The B3LYP/6-31+G(d,p) survey provided a fairly inexpensive method to construct potential energy surfaces for the $O-C_3H_6$ system. Nevertheless, steps for which the reaction coordinate is

more complicated could not be easily characterized using the QST2 method at the B3LYP/6-31+G(d,p) level. Notably, these include reactions for which there is no or a very small potential barrier, such as the initial O + C_3H_6 addition step and singlet-surface homolytic bond dissociation of C_3H_6O intermediates.

On the triplet surface the initial O-atom addition reaction required the additional efforts associated with a relaxed PES scan at the DFT level followed by a G3 IRCMax calculation. The IRCMax calculation uses the DFT geometry for subsequent single point energy calculations rather than a geometry obtained with the MP2 method, which is the normal optimized geometry in the G3 compound calculation. This method assumes that the DFT calculations produce geometries close to those of the actual reaction coordinate and that subsequent higher level single point energy calculations within the compound G3 method based on this geometry provide more accurate energies than does the DFT method by itself.[41]

On the singlet surface, the homolytic bond dissociation reactions were modeled using a relaxed PES with a full unrestricted MP2/6-31G(d) calculation to obtain a minimum energy path. Transition states were found by optimizing a structure near the energy maximum using the Berny algorithm and a full unrestricted MP2/6-31G(d) calculation. The resulting transition state structure could then be used in the remaining G3 calculations to obtain G3 energies.

II.B RRKM methodology

The *Multiwell* suite of programs was used to analyze the reaction rates and branching ratios.[42,43] The *Multiwell* suite contains programs to calculate moments of inertia, internal state sums and densities, reaction rates, and branching ratios. The program is designed to solve the RRKM master equation, described in detail in a number of classic kinetics texts.[44,45] RRKM

theory uses internal state sums (for transition states) and densities (for intermediates) to calculate unimolecular reaction rates. Rotational states are included in the *Multiwell* program, which approximates all molecules as symmetric tops with two equal moments of inertia. This approximation is made by taking the geometric mean of the two most similar moments, input into *Multiwell* as a two-dimensional external moment.

Vibrational wavefunctions and frequencies were obtained from the Gaussian 03 results. The MP2 level of calculation performed as part of the G3 compound method provides the $3N-6 = 24$ vibrational frequencies, less the one imaginary frequency associated with the transition states. The $O-C_3H_6$ system possesses internally hindered rotations, identified through visual inspection of the program animation of the internal mode displacements. For instance, triplet CH_3CH_2CHO has two hindered rotations, the first along the CH_3CH_2-CHO bond and the second along the CH_3-CH_2CHO bond, with symmetries of two and three, respectively. Gaussian 03 treats all internal degrees of freedom as harmonic oscillators, and hindered rotations appear as very low frequency vibrations when thus approximated.

For the hindered rotors the harmonic oscillator assumption results in a grossly inaccurate calculation of the sums of states. These degrees of freedom were treated with the method described by Knyazev for one-dimensional hindered rotors.[46] The Knyazev method calculates sums of rotational states based on the potential barrier to the rotation, V. The sums are calculated from the rotational constant, B (cm^{-1}), the reduced moment of inertia, I_r (amu Å^2), the effective harmonic frequency, ω (cm^{-1}), and the symmetry number n using Eqs. (1) and (2):

$$B = \frac{16.85763}{I_r} \tag{1}$$

$$V = \frac{1}{B}\left[\frac{\omega}{n}\right]^2 \tag{2}$$

The moments of inertia for the two-dimensional external moment and for the two hindered rotors were calculated using the coordinates obtained from the G3 calculations. The coupling between the internal rotors was ignored and they were treated as two independent one-dimensional modes.

Once all the internal degrees of motion were properly assigned, the sums and densities of states were calculated using *Multiwell* routines based on the Stein-Rabinovitch extension to the Beyer-Swinehart algorithm.[47] *Multiwell* uses a two array system, one array for lower energy and a second array for higher energy. A grain size of 10 cm^{-1} with 250 bins was used for the lower energy array for energies from 0 to 2500 cm^{-1} while a grain size of 341.365 cm^{-1} with 250 bins was used for the higher energy array up to 85000 cm^{-1}. The program interpolates values to produce an output with 10 cm^{-1} resolution from 0 to 85000 cm^{-1}. The RRKM master equation was solved using Gillespie's exact stochastic method.[48,49]

For the pressure dependence, the collider was taken to be $CH_3CH(O)CH_2$ (propylene oxide). The Lennard-Jones collision parameters σ and ε/k_B for $CH_3CH(O)CH_2$ were estimated by adding the difference between the values for $CH_2(O)CH_2$ and CH_2CH_2 to those for C_3H_6, resulting in $\sigma = 4.6$ Å and $\varepsilon/k_B = 475$ K. The collisional energy transfer efficiencies were calculated using a monoexponential model[50] with the exponential constant $\alpha = 100 + 0.015*E$ cm^{-1}, where E is the internal energy. Reaction rates and branching ratios in the 300-3000 K temperature and 0.001-760 Torr pressure ranges were investigated, with the assumption that the system is chemically

activated through $O + C_3H_6$ recombination. Note that the internal energy in the $O + C_3H_6$ system at a given temperature can be approximated as

$$E = E_v + E_{R,T} = \sum_j \frac{v_j e^{\frac{-v_j}{kT}}}{1 - e^{\frac{-v_j}{kt}}} + 3kT \tag{3}$$

where the sum is over the vibrational modes j and $3kT$ accounts for the external rotational and translational degrees of freedom. The 300-3000 K temperature range corresponds to a range of 10.6 - 427 kJ mol^{-1} internal energy in the $O + C_3H_6$ system.

III. Results and Discussion

III.A Calculated energy values

The calculated intermediate and transition state energy values for the O-C_3H_6 system are summarized in Tables I and II for the triplet and singlet surfaces, respectively. The B3LYP results are reported for two different basis sets, and with and without zero-point energy correction. The corresponding energy levels are plotted in Fig. 1 (triplet system) and Fig. 2 (singlet system), with solid lines indicating reaction pathways that may or may not be favorable. In the tables and figures, reaction intermediates corresponding to energy minima are denoted by ^{3}INT(i) for the triplet states and ^{1}INT(i) for the singlet states. Likewise, transition states corresponding to first-order energy saddle points are denoted ^{3}TS(i) and ^{1}TS(i) for the triplets and singlets, respectively. The energy zero is defined as the sum of the $O(^3P)$ and C_3H_6 separated reactant energies for both surfaces.

11

III.A.1 Triplet surface

From Fig. 1 it can be seen that the O-C_3H_6 triplet surface is characterized by three bound intermediates, denoted ^{3}INT(1), ^{3}INT(2), and ^{3}INT(3). The initial step involves addition of the O atom to the terminal carbon of the C=C bond in propene, generating the relatively stable secondary carbon biradical ^{3}INT(2). The reaction coordinate is complicated by an initial energy minimum at ^{3}INT(1), which is a weakly bound complex with a <10 kJ mol^{-1} barrier to further rearrangement. The reaction of O + C_3H_6 to form the CH_3CHCH_2O triplet biradical ^{3}INT(2) is therefore effectively without barrier. However, ^{3}INT(1) is important with respect to constructing the RRKM model discussed below.

Fortuitously ^{3}TS(1) was found using the QST2 method during the initial B3LYP/6-31+G(d,p) survey.   The B3LYP/6-311++G(3df,2p) method failed to find ^{3}TS(1) as did the B3LYP/6-311G(2d,d,p) step within the CBS-QB3 method.   Since the CBS-QB3 method optimizes initial geometries with a DFT step, it is not surprising that both the CBS-QB3 and DFT methods can fail to identify difficult saddle points. The G3 method uses a full MP2 step to optimize the initial geometry, with MP2 methods known for their accuracy with respect to transition state geometries. The additional investment of the MP2 step in the G3 method enabled the saddle point to be found.

Following the energy gradient from ^{3}TS(1) leads to the formation of the triplet biradical intermediate ^{3}INT(2). The B3LYP/6-31+G(d,p) and IRCMax calculations of the relaxed PES for CH_3CHCH_2O redissociation to the reactants are shown in Fig. 3 along with illustrations of the associated structures along the reaction coordinate. The IRCMax calculation yields an upper limit for the ^{3}TS(1) energy using the DFT structure, while the ^{3}INT(1) energy is calculated using the more accurate MP2 geometry. Thus, an upper limit for the local energy barrier governing the

rearrangement of the weakly-bound ^{3}INT(1) intermediate is equal to the difference between the ^{3}TS(1) and ^{3}INT(1) energies, or 7.5 kJ mol^{-1}.

Aside from redissociation via the entrance channel, the biradical ^{3}INT(2) has two dissociative pathways leading to products. One pathway leads to $H_2CO + CH_3CH$ via C-C bond cleavage, while the second leads to the formation $H + CH_3CHCHO$ through C-H bond breaking. As can be seen from Fig. 1, the $H + CH_3CHCHO$ pathway has a lower barrier; it is also doubly degenerate as there are two equivalent H atoms which can be lost. In addition, any product H_2CO could conceivably dissociate in a secondary process to $H_2 + CO$. The H_2 and CO products are accessible within the energy limits of the system, but the activation energy associated with the dissociation of H_2CO is calculated to be 338.7 kJ mol^{-1} using the G3 method, effectively eliminating this channel on the triplet surface.

In addition to the two dissociative paths from ^{3}INT(2) there is also the possibility of a 1,2 H-atom shift to form triplet propanal, CH_3CH_2CHO, ^{3}INT(3). However, a very large energy barrier of 122.3 kJ mol^{-1} is calculated for this rearrangement and it is not accessible for thermal reactant energies. For any ^{3}INT(3) that is formed two product channels are available, both involving C-C bond cleavage. Cleavage of the CH_3CH_2-CHO bond is the much lower energy pathway and results in the formation of $HCO + CH_3CH_2$. The competing dissociation, H_3C-$CH_2CHO \rightarrow CH_3 + CH_2CHO$, exhibits an approximately three times larger activation energy.

It is known that the formyl radical HCO is a major product of the $O + CH_3CHCH_2$ reaction. Nevertheless, on the triplet surface only ^{3}INT(3) dissociates to yield HCO as a product. Given the large energy barrier to formation of ^{3}INT(3), any HCO product is likely formed from singlet surface dissociation (see below).

III.A.2 Singlet surface

The O-C_3H_6 singlet surface is also characterized by three bound intermediates, denoted ^{1}INT(1), ^{1}INT(2), and ^{1}INT(3). The first intermediate, propylene oxide, ^{1}INT(1), has a dissociation channel to form $C_2H_4 + H_2CO$. Though the activation energy for further dissociation of H_2CO on the triplet surface is prohibitive, on the singlet surface the barrier (^{1}TS(6)) associated with H_2CO dissociation lies only about 10 kJ mol^{-1} above the O(^{3}P) + C_3H_6 reactant energy. A second pathway involves rearrangement via C(O)C ring opening of ^{1}INT(1) to form singlet propanal CH_3CH_2CHO, ^{1}INT(2).

From ^{1}INT(2), singlet propanal, there are four dissociation/rearrangement pathways in addition to the entrance path. One of the four pathways involves tautomerization to the alcohol $CH_3CHCHOH$, ^{1}INT(3), which can subsequently dissociate to form $H_2O + CH_3CCH$. A second dissociative path from ^{1}INT(2) produces $C_2H_4 + H_2CO$ through a 3,1 H-atom shift. This is the second route to $C_2H_4 + H_2CO$ on the singlet surface, the first resulting from dissociation of the oxide ^{1}INT(1) as discussed above.

The two remaining reaction pathways from ^{1}INT(2) involve homolytic bond cleavage of the C-C bonds to form the radical pairs $C_2H_5 + CHO$ and $CH_3 + CH_2CHO$. Accurately calculating homolytic bond cleavage on a singlet surface is often problematic. Our attempts to locate transition states for these reactions using DFT-level PES surveys were unsuccessful. However, a PES using a full unrestricted MP2/6-31G(d) calculation did pass through a maximum for both dissociation paths. Transition states were found by performing a Berny optimization, using the same full unrestricted MP2/6-31G(d) method, for a structure near the maximum of the PES for each reaction. In both cases a structure was obtained with a single imaginary frequency. The IRCs were followed at the MP2 level in both directions to ensure that the transition state

connected the reactants and products. The transition state structures were then used in the remaining sequence of steps to obtain G3 energies. These transition states are reported as ^{1}TS(7) and ^{1}TS(8) in Table II and Figure 2. The two dissociation pathways have very similar activation energies, in contrast to those for triplet propanal, ^{3}INT(3), for which the pathways display significant differences in activation energy.

It should be noted that repeated stationary state optimization runs using the DFT and MP2 methods starting from the molecular geometry of the triplet biradical failed to locate an analogous open-chain singlet biradical intermediate, ^{1}CH$_3$CHCH$_2$O. Instead the singlet system calculation converges on either the ^{1}INT(2) (aldehyde) or ^{1}INT(3) (enol) geometry. We cannot locate a stable, open-chain singlet biradical, consistent with the computational results of Nguyen et al. [33] and other workers[51] for the singlet PES of C$_2$H$_4$O.

III.B RRKM model

For the purposes of the RRKM calculation, a model of the triplet surface was constructed including two intermediates and five product channels (see Fig. 1). The biradical CH$_3$CHCH$_2$O (^{3}INT(2)) was assigned to the first well and triplet CH$_3$CH$_2$CHO (^{3}INT(3)) to the second well. Four channels arise from the biradical ^{3}INT(2): (1) redissociation to the reactants O + C$_3$H$_6$, (2) a 1,2 H-atom shift to form ^{3}INT(3), and dissociation to yield either (3) H + CH$_3$CHCHO or (4) H$_2$CO + CH$_3$CH. From propanal ^{3}INT(3) there are three reaction paths: (1) rearrangement back to ^{3}INT(2), and dissociation to yield (2) CH$_3$ + CH$_2$CHO or (3) C$_2$H$_5$ + HCO.

Similarly, a model of the singlet surface was constructed with three intermediates and four product channels (Fig. 2). ^{1}INT(1) was assigned to the first well, ^{1}INT(2) to the second, and ^{1}INT(3) to the third. From the first well two reactions are possible, dissociation to yield C$_2$H$_4$ +

H$_2$CO and rearrangement to form ^{1}INT(2). ^{1}INT(2) can (1) rearrange via a 2,1 H-atom shift and ring closure to form ^{1}INT(1), (2) tautomerize to the enol isomer CH$_3$CHCHOH, ^{1}INT(3), (3) undergo a 3,1 H-atom shift and C-C bond scission to form C$_2$H$_4$ + H$_2$CO, or (4) dissociate along one of its C-C bonds to produce the radical pairs C$_2$H$_5$ + HCO or CH$_3$ + CH$_2$CHO. Of the reactions described above, the dissociation pathways producing the HCO and CH$_2$CHO radicals are thought to be dominant.[4] Secondary reactions involving the dissociation of HCO to H + CO[52] and the dissociation of the vinoxy radical CH$_2$CHO to several different products have also been studied.[5,53] From the third well ^{1}INT(3), in addition to the entrance channel there is one product channel to form CH$_3$CCH + H$_2$O. The model was run under the same conditions (pressure, temperature, and collisional relaxation parameters) as described above for the triplet surface, with two exceptions: (1) the reactants were taken to have a "thermal" energy distribution rather than a "chemically activated" distribution because we had no activating channel to reference, with the same O(^{3}P) + C$_3$H$_6$ energy zero, and (2) the G3 energy results were used directly.

On both surfaces, rearrangements between intermediates were allowed to be reversible while dissociative reactions were assumed to be irreversible.

III.B.1 Branching ratios on the triplet surface

The results of the RRKM calculation for the triplet surface model appear in Table III for the 300-3000 K temperature range and high (760 Torr) and low (0.001 Torr) pressure. Pressure was found to have little influence over the branching ratios, suggesting that the vibrational self-relaxation rates for $p \leq 1$ atm are negligible compared to the triplet intermediate inverse lifetimes.

For reactant internal energies greater than 20.2 kJ mol^{-1} there is sufficient energy to overcome the barrier to convert ^{3}INT(2) to ^{3}INT(3) by the 1,2 H-atom shift. Yet, even at the highest temperature of 3000 K, with equipartition suggesting that each vibrational mode has up to 24.9 kJ mol^{-1} energy, products resulting from the dissociation of ^{3}INT(3) are very minor, about 2.5%. It appears that nearly all the dissociation products from the triplet surface result from the dissociation of the biradical ^{3}INT(2). Nguyen *et al.* obtained similar results for the O + C$_2$H$_4$ system.[33]

For the reactions of the triplet biradical, CH$_3$CHCH$_2$O (^{3}INT(2)), the activation barrier is lowest for H-atom loss to form H + CH$_3$CHCHO and highest for the 1,2 H-atom shift to form triplet CH$_3$CH$_2$CHO (^{3}INT(3)). The curvature of the PES in the vicinity of the transition state also strongly influences the reaction rate. Given that the reaction rate is proportional to the transition state sum of states, a faster rate is predicted for a PES with less curvature and a larger internal state sum. As an indication of this effect, Fig. 4 shows the computed sums of states for the ^{3}TS(2), ^{3}TS(3), and ^{3}TS(4) transition states from threshold to 23.9 kJ mol^{-1} (2000 cm^{-1}) above the respective transition state energy. It can be seen that the ^{3}TS(3) state possesses about 6× as many internal states as ^{3}TS(2) or ^{3}TS(4) at any given excess energy. The H + CH$_3$CHCHO product channel dominates at low temperature via the low threshold energy transition state ^{3}TS(4). However, the higher energy path producing CH$_3$CH + H$_2$CO becomes dominant as the temperature (or energy) increases and the ^{3}TS(3) internal state sum rapidly becomes greater than that for ^{3}TS(4). (Consider as an analogy water held back by a dam; the water level connotes energy, while the dam connotes an energy barrier. For low levels the water leaks through a small hole in the dam − analogous to the formation of H + CH$_3$CHCHO − while for high levels the

water flows much faster over the top of the dam – analogous to the formation of H_2CO + CH_3CH.)

The RRKM analysis shows that rearrangement of [3]INT(2) to [3]INT(3) on the triplet surface is not favored even in the presence of significant excess energy. However, intersystem crossing of [3]INT(2) from the triplet surface to the singlet surface may occur. Our *ab initio* work has shown that for singlet CH_3CHCH_2O the 1,2 H-atom shift exhibits a small or no barrier, similar to others'[33] findings for singlet CH_2CH_2O. (Recall the discussion above that the calculations could not identify a bound CH_3CHCH_2O singlet intermediate.) Intersystem crossing of [3]INT(2) to the singlet surface would then result in the formation of singlet CH_3CH_2CHO, [1]INT(2), which can undergo several different rearrangements or directly dissociate as described below. On the triplet surface HCO can only be formed through dissociation of [3]INT(3), which according to our RRKM analysis is a minor channel at best. Instead, any HCO product is likely formed from dissociation of [1]INT(2) following intersystem crossing.

III.B.2 Branching ratios on the singlet surface

Table IV lists the singlet surface product branching ratios for the same 300-3000 K temperature range and for 760, 0.5, and 0.001 Torr pressure. The low-temperature dissociation is dominated by the formation of C_2H_4 + H_2CO, with the formation of the C_2H_5/HCO and CH_3/CH_2CHO radical pairs quickly becoming dominant as the temperature increases. The H_2O + CH_3CCH product channel arising from the enol $CH_3CHCHOH$ ([1]INT(3)) intermediate does not occur at any temperature. From Fig. 2 it would seem reasonable to assume that the C_2H_4 + H_2CO and H_2O + CH_3CCH product channels would be at least as probable as the C_2H_5 + HCO and CH_3 + CH_2CHO channels at high temperature based on energy barrier considerations.

However, the corresponding transition state sums exhibit a two to three order-of-magnitude advantage for the C-C bond dissociation pathways compared to the other pathways. Thus, the alkyl-aldehyde radical pairs dominate the high-temperature product yield for the same reasons described in section III.B.1 for the dissociation of ^{3}INT(2). Note that for the lower temperatures (≤ 600 K) and atmospheric pressure (760 Torr) much of the energized CH_3CH_2CHO intermediate population is stabilized by collisions prior to rearrangement or dissociation. With the 760-Torr collision rate calculated as 1.46×10^{10} s^{-1} and half of the CH_3CH_2CHO stabilized, the 300-K chemically-activated lifetime is estimated to be on the order of 100 ps or larger.

III.C Summary of RRKM branching ratios

Table V summarizes the major product distribution from both surfaces at low (300 K) and high (≥ 2000 K) temperatures. For the triplet surface, the H + CH_3CHCHO product channel dominates, with a significant contribution from the $H_2CO + CH_3CH$ channel at high temperature. For the singlet surface, $H_2CO + C_2H_4$ is the principal product channel at low temperature, with the C_2H_5/HCO and CH_3/CH_2CHO radical pairs the nearly exclusive products at high temperature. Formaldehyde (H_2CO) may arise from either the singlet or triplet surfaces, though it is likely to be produced from the singlet surface at low temperature and from the triplet surface at high temperature. The presence of CH_3CH or C_2H_4 coproduct could conceivably be used as an indication of the source of H_2CO, CH_3CH indicating triplet surface dissociation and C_2H_4 indicating singlet surface dissociation.

IV. Summary

The lowest lying triplet and singlet potential energy surfaces for the $O + C_3H_6$ reaction have been characterized using the DFT and *ab initio* CBS-QB3 and G3 theoretical methods. With the intermediate and transition state energies, geometries, and vibrational frequencies as inputs, RRKM statistical theory was then used to predict product branching fractions as a function of reactant temperature and pressure. The potential energy surface for the $O + C_3H_6$ reaction is similar to that reported by Nguyen *et al.* for the $O + C_2H_4$ system,[33] but for the additional features associated with H-atom transfers and C-C bond cleavage involving the extra C_3H_6 carbon atom. In both systems, products arise from reactions of the initially-formed CH_3CHCH_2O or CH_2CH_2O biradical. Rearrangement of the nascent triplet biradical CH_3CHCH_2O to CH_3CH_2CHO (propanal) is hindered both by a large activation energy barrier and by a low sum of states for the transition state. The triplet system yields mostly $H + CH_3CHCHO$ products at all temperatures. The nascent singlet biradical CH_3CHCH_2O, accessed through intersystem crossing, quickly rearranges to singlet propanal. Subsequent singlet surface dissociation yields mostly $C_2H_4 + H_2CO$ at low temperature and a roughly 1:1 proportion of $C_2H_5 + HCO$ and $CH_3 + CH_2CHO$ at high temperature. Aside from evidence that singlet CH_3CH_2CHO is stabilized at 1 atm at low temperature, pressure was found to have little influence over the branching ratios, suggesting that the vibrational self-relaxation rates for $p \leq 1$ atm are negligible compared to the dissociation rates.

References

(1)   *Gas-phase combustion chemistry*; Gardiner, W. C., Ed.; Springer: New York, 2000, pp 543.

(2)   Linan, A.; Williams, F. A. *Fundamental Aspects of Combustion*; Oxford University Press, 1993.

(3)   Cvetanović, R. J. *Adv. Photochem.* **1963**, *1*, 115.

(4)   Quandt, R.; Min, Z.; Wang, X.; Bersohn, R. *J. Phys. Chem. A* **1998**, *102*, 60.

(5)   Su, H.; Bersohn, R. *J. Phys. Chem. A* **2001**, *105*, 9178.

(6)   Casavecchia, P.; Capozza, G.; Segoloni, E.; Leonori, F.; Balucani, N.; Volpi, G. G. *J. Phys. Chem. A* **2005**, *109*, 3527.

(7)   Morton, M. L.; Szpunar, D. E.; Butler, L. J. *J. Chem. Phys.* **2001**, *115*, 204.

(8)   Schmoltner, A. M.; Chu, P. M.; Brudzynski, R. J.; Lee, Y. T. *J. Chem. Phys.* **1989**, *91*, 6926.

(9)   Hedin, A. E. *J. Geophys. Res.* **1991**, *96*, 1159.

(10)   Bernstein, L. S.; Elgin, J. B.; Pike, C. P.; Knecht, D. J.; Murad, E.; Zehnpfennig, T. F.; Galica, G. E.; Stair, A. T., Jr. *J. Geophys. Res.* **1996**, *101*, 383.

(11)   Murad, E. *J. Spacecr. Rockets* **1996**, *33*, 131.

(12)   Upschulte, B. L.; Caledonia, G. E. *Journal of Chemical Physics* **1992**, *96*, 2025.

(13)   Orient, O. J.; Chutjian, A.; Murad, E. *J. Chem. Phys.* **1994**, *101*, 8297.

(14)   Orient, O. J.; Chutjian, A.; Murad, E. *Phys. Rev. A* **1995**, *51*, 2094.

(15)   Upshulte, B. L.; Oakes, D. B.; Caledonia, G. E.; Blumberg, W. A. M. *Geophysical Research Letters* **1992**, *19*, 993.

(16)   Oakes, D. B.; Sonnenfroh, D. M.; Caledonia, G. E.; Blumberg, W. A. M. *J. Geophys. Res.* **1994**, *99*, 23249.

(17)   Banks, B. A.; Snyder, A.; Miller, S. K.; de Groh, K. K.; Demko, R. *J. Spacecr. Rockets* **2004**, *41*, 335.

(18)   Bley, U.; Dransfeld, P.; Himme, B.; Koch, M.; Temps, F.; Wagner, H. G. "Primary products of the reaction between $O(^3P)$-atoms and C_2H_4 studied with esr- and lmr-detection"; Twenty-Second Symposium (International) on Combustion, 1988.

(19)   Endo, Y.; Tsuchiya, S.; Yamada, C.; Hirota, E. *J. Chem. Phys.* **1986**, *85*, 4446.

(20)   Knyazev, V. D.; Arutynov, V. S.; Vedeneev, V. I. *Int. J. Chem. Kin.* **1992**, *24*, 545.

(21)   Dodd, J. A.; Hwang, E. S.; Castle, K. J.; DeBoer, G. D. *J. Phys. Chem. A* **2004**, *108*, 10965.

(22)   Gardner, J. L.; Miller, S. M. *J. Chem. Phys.* **2004**, *121*, 5920.

(23)   Koda, S.; Endo, Y.; Tsuchiya, S.; Hirota, E. *J. Phys. Chem.* **1991**, *95*, 1241.

(24)   Oguchi, T.; Ishizaki, A.; Kakuta, Y.; Matsui, H.; Miyoshi, A. *J. Phys. Chem. A* **2004**, *108*, 1409.

(25)   Min, Z.; Wong, T.-H.; Quandt, R.; Bersohn, R. *J. Phys. Chem. A* **1999**, *103*, 10451.

(26)   Min, Z.; Wong, T.-H.; Su, H.; Bersohn, R. *J. Phys. Chem. A* **2000**, *104*, 9941.

(27)   Su, H.; Bersohn, R. *J. Chem. Phys.* **2001**, *115*, 217.

(28)   Abou-Zied, O. K.; McDonald, J. D. *J. Chem. Phys.* **1998**, *109*, 1293.

(29)   Foner, S. N.; Hudson, R. L. *J. Chem. Phys.* **1968**, *49*, 3724.

(30)   Foner, S. N.; Hudson, R. L. *J Chem Phys* **1970**, *53*, 4377.

(31)   Kanofsky, J. R.; Gutman, D. *Chem. Phys. Lett.* **1972**, *15*, 236.

(32)   Kleinermanns, K.; Luntz, A. C. *J. Phys. Chem.* **1981**, *85*, 1966.

(33)   Nguyen, T. L.; Vereecken, L.; Hou, X. J.; Nguyen, M. T.; Peeters, J. *J. Phys. Chem. A* **2005**, *109*, 7489.

(34)   Jursic, B. S. *Journal of Molecular Structure (Theochem)* **1999**, *492*, 85.

(35)   Foresman, J. B.; Frisch, A. *Exploring chemistry with electronic structure methods*; Gaussian, Inc.: Pittsburgh, 1996.

(36)   Montgomery, J. A., Jr.; Frisch, M. J.; Ochterski, J. W.; Petersson, G. A. *J. Chem. Phys.* **1999**, *110*, 2822.

(37)   Curtiss, L. A.; Raghavachari, K.; Redfern, P. C.; Rassolov, V.; Pople, J. A. *J. Chem. Phys.* **1998**, *109*, 7764.

(38)   Stephens, P. J.; Devlin, F. J.; Chabalowski, C. F.; Frisch, M. J. *J. Phys. Chem. A* **1994**, *98*, 11623.

(39)   Schlegel, H. B. *Adv. Chem. Phys.* **1987**, *67*, 249.

(40)   Montgomery, J. A., Jr.; Frisch, M. J.; Ochterski, J. W. *J. Chem. Phys.* **2000**, *112*, 6532.

(41)   Malick, D. K.; Petersson, G. A.; Montgomery, J. A., Jr. *J. Chem. Phys.* **1998**, *108*, 5704.

(42)   Barker, J. R. *Int. J. Chem. Kin.* **2001**, *33*, 232.

(43)   Barker, J. R. MultiWell-2.0 software, 2006; University of Michigan, 2006.

(44)   Baer, T.; Hase, W. L. *Unimolecular Reaction Dynamics: Theory and Experiments*; Oxford University Press: New York, 1996.

(45)   Holbrook, K. A.; Pilling, M. J.; Robertson, S. H. *Unimolecular Reactions*; John Wiley & Sons: Chichester, 1996.

(46)   Knyazev, V. D. *J. Phys. Chem. A* **1998**, *102*, 3916.

(47)   Stein, S. E.; Rabinovitch, B. S. *J. Chem. Phys.* **1973**, *58*, 2438.

(48)   Gillespie, D. T. *J. Comp. Phys.* **1976**, *22*, 403.

(49)   Gillespie, D. T. *J. Comp. Phys.* **1978**, *28*, 395.

(50)   Barker, J. R.; Yoder, L. M.; King, K. D. *J. Phys. Chem. A* **2001**, *105*, 796.

(51)   Smith, B. J.; Nguyen, M. T.; Bouma, W. J.; Radom, L. *J. Amer. Chem. Soc.* **1991**, *113*, 6452.

(52)   Neyer, D. W.; Kable, S. H.; Loison, J.-C.; Houston, P. L.; Burak, I.; Goldfield, E. M. *J. Chem. Phys.* **1992**, *97*, 9036.

(53)   Osborn, D. L.; Choi, H.; Mordaunt, D. H.; Bise, R. T.; Neumark, D. M. *J. Chem. Phys.* **1997**, *106*, 3049.

Table I. Triplet surface *ab initio* energies (kJ mol^{-1}, 0 K) relative to O(^{3}P) + CH$_3$CHCH$_2$ (^{1}A), computed using the B3LYP (two different basis sets), CBS-QB3, and G3 methods. For the blank entries the structure and energy could not be determined.

Species		B3LYP				CBS-QB3	G3
		6-31+(d,p)		6-311 ++(3df,2p)			
		w/o ZPE	w/ ZPE	w/o ZPE	w/ ZPE		
O(^{3}P) + CH$_3$CHCH$_2$ (^{1}A)		0.0	0.0	0.0	0.0	0.0	0.0
O(^{3}P) + CH$_3$CHCH$_2$ (^{1}A)	^{3}INT(1)						-12.3
CH$_3$CHCH$_2$O (^{3}A)	^{3}INT(2)	-123.5	-124.2	-123.8	-125.0	-104.3	-99.8
CH$_3$CH$_2$CHO (^{3}A)	^{3}INT(3)	-148.7	-144.2	-151.3	-147.4	-127.3	-124.3
CH$_3$CH (^{3}A) + H$_2$CO (^{1}A')		-23.2	-38.3	-30.7	-46.4	-30.1	-29.2
CH$_3$CHCHO (^{2}A) + H(^{2}S)		-62.5	-85.1	-71.9	-94.7	-84.4	-78.3
CH$_3$ (^{2}A)+ CH$_2$CHO (^{2}A")		-113.6	-132.5	-120.7	-139.9	-114.9	-115.1
CH$_3$CH$_2$ (^{2}A') + HCO (^{2}A')		-105.0	-124.0	-116.6	-135.9	-111.5	-111.3
CH$_3$CH (^{3}A) + H$_2$($^1\Sigma_g$) + CO($^1\Sigma_g$)		17.9	-27.3	2.6	-41.4	-29.9	-25.4
Saddle points	^{3}TS(1)	-24.7	-23.6				-4.8
	^{3}TS(2)	7.7	-1.8	3.2	-7.2	18.4	22.1
	^{3}TS(3)	-22.9	-32.0	-29.1	-38.8	-23.2	-20.4
	^{3}TS(4)	-45.4	-62.6	-51.1	-68.5	-50.8	-43.5
	^{3}TS(5)	-7.8	-17.7	-14.3	-24.7	10.8	16.9
	^{3}TS(6)	-84.7	-90.2	-104.1	-109.6	-81.6	-87.7

Table II. Singlet surface *ab initio* energies (kJ mol^{-1}, 0 K) relative to O(^{3}P) + CH$_3$CHCH$_2$ (^{1}A) computed using the B3LYP (two different basis sets), CBS-QB3, and G3 methods. For the blank entries the structure and energy could not be determined.

Species		B3LYP 6-31+(d,p) w/o ZPE	B3LYP 6-31+(d,p) w/ ZPE	B3LYP 6-311 ++(3df,2p) w/o ZPE	B3LYP 6-311 ++(3df,2p) w/ ZPE	CBS-QB3	G3
CH$_2$CH$_2$ (^{1}A$_g$) + H$_2$CO (^{1}A′)		-317.1	-322.0	-330.9	-336.1	-333.3	-328.3
CH$_3$CH(O)CH$_2$ (^{1}A)	^{1}INT(1)	-357.1	-341.8	-362.6	-347.3	-365.0	-358.1
CH$_3$CH$_2$CHO (^{1}A′)	^{1}INT(2)	-450.6	-438.1	-456.4	-444.3	-454.1	-449.6
CH$_3$CHCHOH (^{1}A)	^{1}INT(3)	-410.1	-397.2	-421.9	-408.6	-419.2	-415.0
CH$_3$CCH + H$_2$O (^{1}A$_1$)		-291.0	-298.2	-314.2	-320.8	-329.1	-326.1
CH$_2$CH$_2$ (^{1}A$_g$) + H$_2$(^{1}Σ$_g$) + CO(^{1}Σ$_g$)		-276.0	-311.1	-297.6	-331.0	-343.6	-337.9
Saddle points	^{1}TS(1)	-31.3	-32.9	-37.7	-39.7	-39.8	-36.6
	^{1}TS(2)	-113.7	-114.1	-117.9	-118.6	-139.1	
	^{1}TS(3)	-120.2		-129.4	-129.6	-124.4	-112.2
	^{1}TS(4)	-163.6	-167.1	-169.3	-173.1	-173.8	-169.2
	^{1}TS(5)	-69.3	-76.4	-79.7	-87.1	-85.9	-79.6
	^{1}TS(6)	47.6	21.7	21.6	-4.7	11.5	10.4
	^{1}TS(7)						-80.6
	^{1}TS(8)						-90.3

Table III. Percent product distribution for triplet CH_3CHCH_2O dissociation channels with yield $\geq 0.5\%$, computed at two different pressures using the RRKM model described in the text.

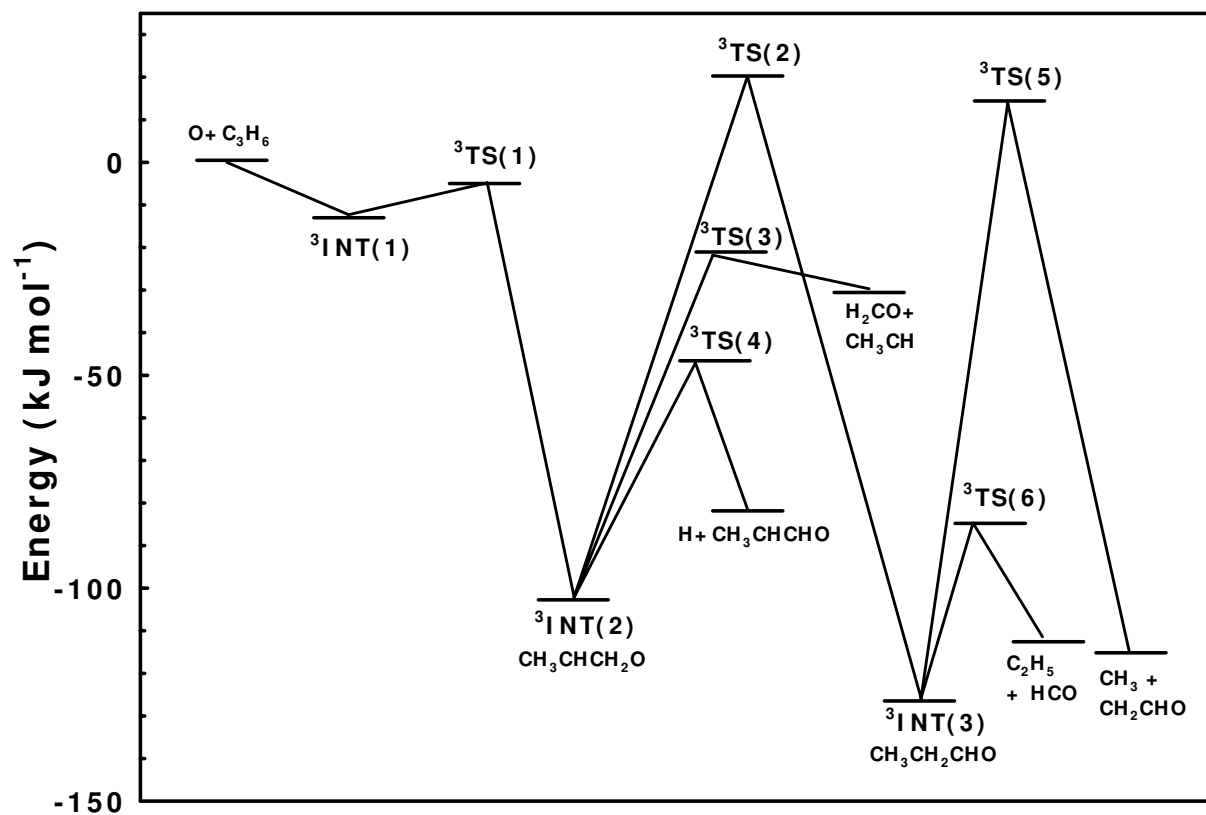| T (K)	760 Torr				0.001 Torr			
	H + CH_3CHCHO	H_2CO + CH_3CH	O + CH_3CHCH_2	C_2H_5 + HCO	H + CH_3CHCHO	H_2CO + CH_3CH	O + CH_3CHCH_2	C_2H_5 + HCO
300	95.3	4.7	0.0	0.0	94.7	5.3	0.0	0.0
600	89.8	10.2	0.0	0.0	89.2	10.7	0.2	0.0
900	84.3	15.4	0.3	0.0	84.0	15.6	0.3	0.1
1200	79.3	19.9	0.7	0.2	79.1	20.1	0.7	0.1
1500	75.8	22.9	1.0	0.3	75.1	23.6	1.0	0.3
1800	72.8	25.3	1.4	0.5	73.3	24.9	1.4	0.5
2100	70.9	26.6	1.6	0.8	71.3	26.0	1.8	0.8
2400	69.0	27.6	2.1	1.2	69.6	26.9	2.4	1.1
2700	68.3	27.4	2.4	1.7	68.3	27.6	2.5	1.5
3000	66.9	27.7	3.0	2.1	66.9	28.1	3.1	1.9

Table IV. Percent product distribution for singlet CH_3CH_2CHO dissociation channels, computed at three different pressures using the RRKM model described in the text. The three principal product channels are shown.

| T (K)	760 Torr[a]			0.5 Torr			0.001 Torr		
	H_2CO + C_2H_4	C_2H_5 + HCO	CH_3 + CH_2CHO	H_2CO + C_2H_4	C_2H_5 + HCO	CH_3 + CH_2CHO	H_2CO + C_2H_4	C_2H_5 + HCO	CH_3 + CH_2CHO
300	36.9	6.5	8.3	56.5	20.7	22.8	56.4	19.8	23.8
600	35.1	27.8	28.4	32.7	33.4	33.9	31.5	34.4	34.2
900	15.3	43.6	40.3	13.8	45.4	40.8	13.8	44.2	42.0
1200	4.7	52.5	42.7	4.8	52.3	42.9	5.0	51.9	43.0
1500	1.9	54.1	44.0	2.1	55.1	42.8	2.0	54.4	43.6
1800	0.8	55.3	43.8	0.7	56.0	43.2	0.8	56.1	43.1
2100	0.7	56.6	42.7	0.5	56.5	43.0	0.4	56.3	43.2
2400	0.6	56.7	42.7	0.6	57.7	41.7	0.4	56.7	42.8
2700	0.6	57.0	42.3	0.6	57.7	41.7	0.7	56.9	42.5
3000	1.0	56.6	42.4	1.0	57.2	41.7	1.1	56.2	42.7

[a]At atmospheric pressure 48.3%, 8.8%, and 0.8% of the energized CH_3CH_2CHO intermediate is stabilized prior to dissociation at temperatures of 300, 600, and 900 K, respectively.

Table V. Percent product distribution for C_3H_6O triplet and singlet dissociation channels for two temperatures, computed at 0.001 Torr using the RRKM model described in the text. The principal product channels are shown.

| T (K)	Triplet surface			Singlet surface		
	H + CH$_3$CHCHO	H$_2$CO + CH$_3$CH	C$_2$H$_5$ + HCO	H$_2$CO + C$_2$H$_4$	C$_2$H$_5$ + HCO	CH$_3$ + CH$_2$CHO
300	95	5	0	57	20	23
≥ 2000	70	28	2	1	56	43

Figure 1. Schematic C_3H_6O triplet surface intermediate and transition state energies and reaction pathways, referenced to E = 0 kJ mol^{-1} for the $O(^3P) + C_3H_6$ separated reactants. The energy values were taken as the average of the CBS-QB3 and G3 energies tabulated in Table I.
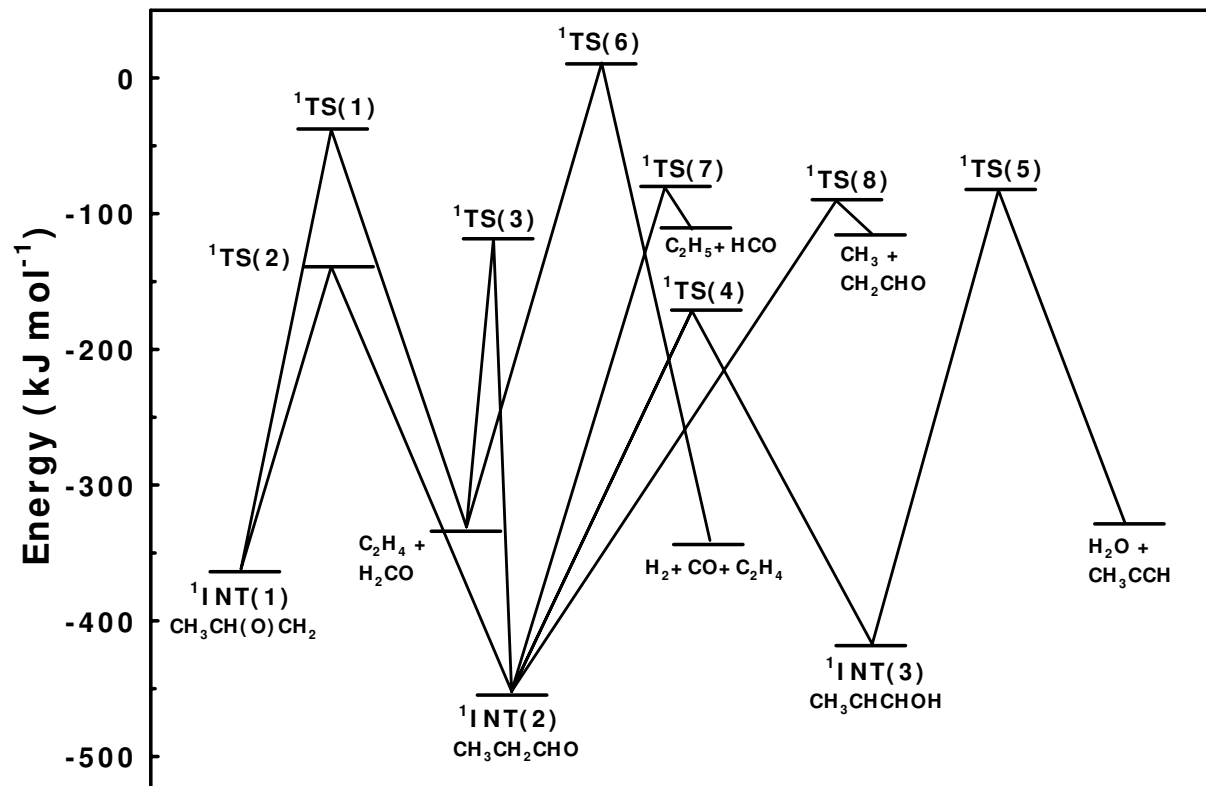
Figure 2. Schematic C_3H_6O singlet surface intermediate and transition state energies and reaction pathways, referenced to $E = 0$ kJ mol^{-1} for the $O(^3P) + C_3H_6$ separated reactants. The energy values were taken as the average of the CBS-QB3 and G3 energies tabulated in Table II.
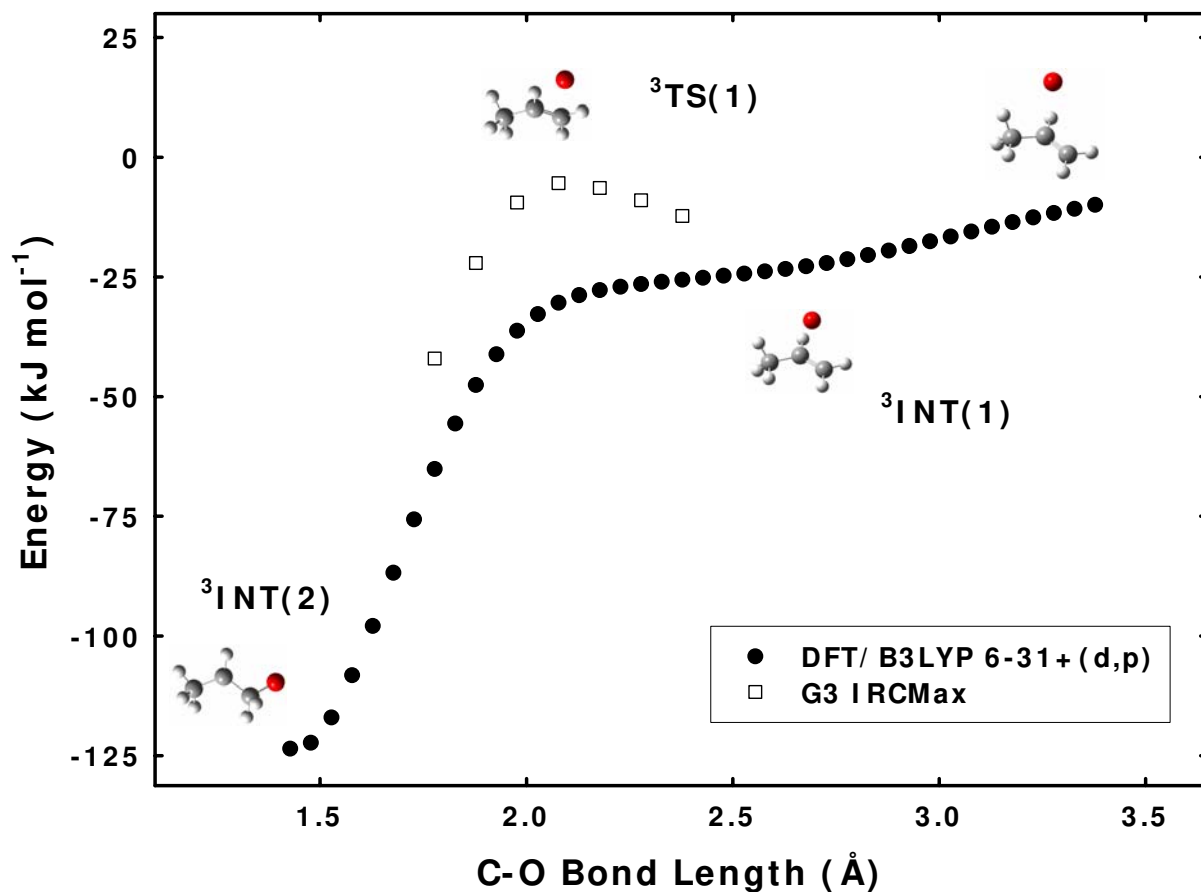
Figure 3. Potential energy profile for redissociation of triplet CH_3CHCH_2O to $O(^3P)$ + C_3H_6, with the other degrees of freedom relaxed as the terminal C-O bond length is increased. Calculations were performed at the B3LYP level with a 6-31+(d,p) basis set, and by the G3 IRCMax method for geometries near the transition state $^3TS(1)$. The energies are relative to the energy of the separated $O(^3P)$ + C_3H_6 reactants.
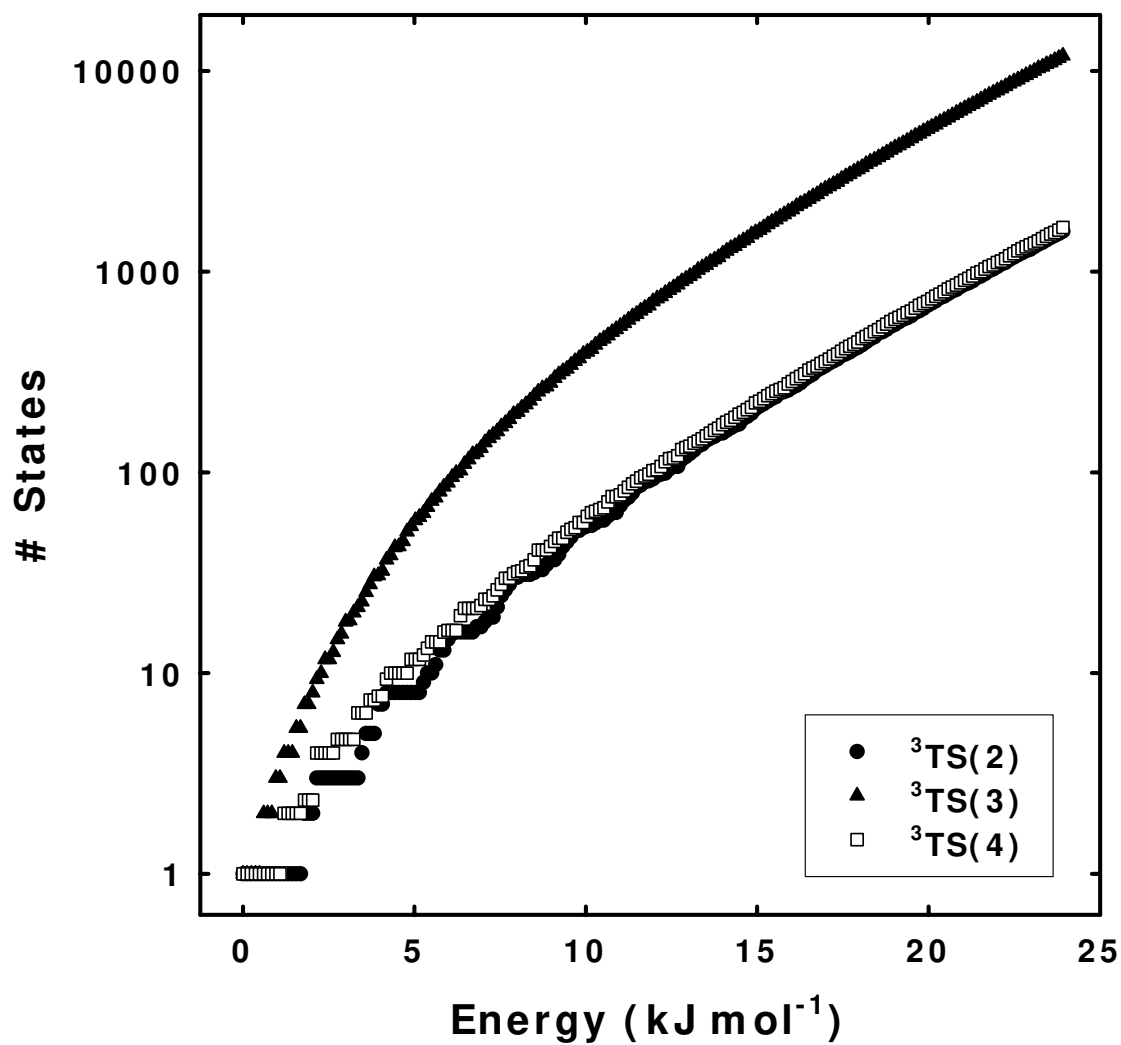
Figure 4. Semi-log plot for three triplet transition state sums as a function of energy above threshold, governing the dissociation of the triplet biradical CH_3CHCH_2O, $^3INT(2)$. The larger $^3TS(3)$ state sums lead to an enhancement of the $H_2CO + CH_3CH$ channel as the energy increases. See Fig. 1 for transition state definitions.